Quasisymmetric and asymmetric gap solitons in linearly coupled Bragg gratings with a phase shift

Yossi J. Tsofe and Boris A. Malomed
Department of Interdisciplinary Studies, School of Electrical Engineering, Faculty of Engineering, Tel Aviv University, Tel Aviv 69978, Israel

(Received 16 July 2006; revised manuscript received 22 February 2007; published 4 May 2007)

We introduce a model including two linearly coupled Bragg gratings, with a mismatch (phase shift θ) between them. The model may be realized as parallel-coupled fiber Bragg gratings (FBGs), or, in the spatial domain, as two parallel planar waveguides carrying diffraction gratings. The phase shift induced by a shear stress may be used to design a different type of FBG sensor. In the absence of the mismatch, the symmetry-breaking bifurcation of gap solitons (GSs) in this model was investigated before. Our objective is to study how mismatch θ affects families of symmetric and asymmetric GSs, and the bifurcation between them. We find that the system's band gap is always filled with solitons (for $\theta \neq 0$, the gap's width does not depend on coupling constant λ if it exceeds some minimum value). The largest velocity of the moving soliton, $c_{\max}$, is found as a function of θ and λ ($c_{\max}$ grows with θ). The mismatch transforms symmetric GSs into *quasisymmetric* (QS) ones, in which the two components are not identical, but their peak powers and energies are equal. The mismatch also breaks the spatial symmetry of the GSs. The QS solitons are stable against symmetry-breaking perturbations as long as asymmetric (AS) solutions do not exist. If θ is small, AS solitons emerge from their QS counterparts through a supercritical bifurcation. However, the bifurcation may become *subcritical* at larger θ. The condition for the stability against oscillatory perturbations (unrelated to the symmetry breaking) is essentially the same as in the ordinary FBG model: both QS and AS solitons are stable if their intrinsic frequency is positive (i.e., in a half of the band gap).

DOI: 10.1103/PhysRevE.75.056603 PACS number(s): 42.81.Dp, 42.50.Md, 42.65.Tg, 05.45.Yv

I. INTRODUCTION

Light propagation in waveguides with a resonant periodic modulation of the refractive index, i.e., Bragg or diffraction gratings, has been a subject of intensive fundamental and applied studies. Fiber Bragg gratings (FBGs) are used in a broad range of applications, such as fiber sensors, optical filters and dispersion compensators, pulse compressors, etc. [1]. The linear coupling between counterpropagating waves induced by the FBG (in the temporal domain) [2], or by a diffraction grating (in the spatial domain) [3], gives rise to a band gap in the system's linear spectrum, while the material nonlinearity of the waveguide populates it with families of solitary waves, known as *gap solitons* (GSs), whose intrinsic frequency belongs to the band gap [2,4]. Solitons in FBGs may also be found outside the band gap, therefore they are called, more generally, Bragg solitons.

Temporal-domain Bragg solitons were originally created in a 6-cm-long piece of an optical fiber with the grating written in its cladding [5]. The smallest velocity of the solitons created in the first experiments was $\simeq 0.5$ of the group velocity of light [6], but very recent observations demonstrate a possibility to drastically reduce the velocity (at least, to 0.16), in *apodized* FBGs [7].

Another species of GSs was predicted in a model of two parallel-coupled FBGs [8], featuring a *symmetry breaking* in two-component GSs. Originally, the symmetry breaking of solitons in linearly coupled systems was predicted in an ordinary dual-core fiber [9]. The main finding was that, with the increase of the soliton's energy E at a fixed strength of the intercore linear coupling, the symmetric soliton becomes unstable at a critical value of E, giving rise to a pair of asymmetric (AS) solitons, which are mirror images to each other. A peculiarity of this bifurcation is that it is slightly *subcritical* (the branches of the AS solutions emerge as unstable ones, going backward in E, but quickly reach a turning point and continue in the forward direction; while passing the turning point, they become stable). Accordingly, there is a narrow interval of bistability and hysteresis involving symmetric and asymmetric solitons, between the above-mentioned turning and bifurcation points.

In Ref. [8], a similar symmetry-breaking bifurcation was predicted for GSs in the model of the dual-core FBG. It is a *supercritical* bifurcation, which gives rise to stable forward-going branches of the AS solitons.

While fabrication of a dual-core fiber grating has been reported [10], a promising setting for the realization of two-core gratings is provided by photonic-crystal fibers (PCFs). They can be easily drawn with one or more relatively wide hollow conduits (creation of PCFs with two such parallel cores has been reported [11]). Then one can write a grating on the inner surface of the conduits. If the band-gap-guiding properties of the PCF are engineered so as to confine the guided mode to a vicinity of the surface of the hollow core, a PCF with two such cores will emulate a dual-core FBG.

Gratings in the dual-core system may be, obviously, written with a mismatch (phase shift) between them. Thus far, this possibility was not considered (except for Ref. [12], where a planar multicore grating was proposed, with a phase shift of π between adjacent cores). The objective of the present work is to consider two-component solitons in the dual-core grating with arbitrary phase shift θ between the cores. In this case, we demonstrate that the model supports *quasisymmetric* (QS) solitons, as a result of deformation of

the symmetric solitons in the system with $\theta=0$. Accordingly, the above-mentioned symmetry-breaking bifurcation, well known for $\theta=0$, has its counterpart in the mismatched system, giving rise to AS solitons, which are drastically different from the QS ones. A difference induced by finite θ is transformation of the supercritical bifurcation into a *subcritical* one.

The Bragg solitons predicted in the paper are possible in a range of parameters where the Bragg-reflection length x_B and the intercore coupling length x_c are on the same order of magnitude. Typically, the FBG has $x_B \sim 1$ mm, which is a realistic value too for x_c in usual dual-core fibers. The respective nonlinearity length should obey the same estimate. With the usual value of the nonlinearity coefficient of the single-mode silica fiber, $\sim 2\ (\mathrm{km\ W})^{-1}$, the latter condition implies that one needs to create a pulse with the peak power about 1 MW. Actually, experiments in fibers may be run at peak powers of up to ~ 10 MW [5]. According to these estimates, the necessary length of the dual-core FBG is no more than 10 cm.

The mismatch in the dual-core FBG may also find an application in the form of a grating-based differential-stress sensor. Indeed, a longitudinal shear stress may easily induce the local mismatch. Even without the intention to use solitons, results for the spectrum of the mismatched dual-core FBG, reported in this paper, provide for a basis to design such sensors.

The present work is focused on the breaking of the (quasi) symmetry of solitons in dual systems with the linear coupling. Under different conditions, symmetry breaking was also studied in two-wave systems with nonlinear (*XPM*) coupling between the components. In particular, it was experimentally demonstrated in an optical fiber that a double-humped soliton, built of two components with orthogonal circular polarizations, one of which is even and the other one odd, features a symmetry-breaking transition to an ordinary single-humped two-component soliton, as the original double-humped one is unstable [13].

The paper is organized as follows. In Sec. II, we formulate the model and outline its two physical realizations, in the temporal and spatial domains. In this section, we also find, in an analytical form, the linear spectrum of the system, and identify the corresponding band gap. In Sec. III, we find families of numerical solutions for solitons of both QS and AS types, and bifurcations which link them are identified in Sec. IV. Stability of the stationary solitons is tested by direct simulations in Sec. V. Conclusions concerning the stability are quite simple. The paper is concluded by Sec. VI.

II. MODEL AND ITS LINEAR SPECTRUM

A. Formulation of the model

The model describing a dual-core FBG was introduced in Ref. [8]. It is based on the following equations in the normalized form (in Ref. [8], it was introduced with $\theta=0$):

$$i(u_1)_t + i(u_1)_x + (|u_1|^2/2 + |v_1|^2)u_1 + v_1 + \lambda u_2 = 0, \quad (1)$$

$$i(v_1)_t - i(v_1)_x + (|v_1|^2/2 + |u_1|^2)v_1 + u_1 + \lambda v_2 = 0, \quad (2)$$

$$i(u_2)_t + i(u_2)_x + (|u_2|^2/2 + |v_2|^2)u_2 + e^{i\theta/2}v_2 + \lambda u_1 = 0, \quad (3)$$

$$i(v_2)_t - i(v_2)_x + (|v_2|^2/2 + |u_2|^2)v_2 + e^{-i\theta/2}u_2 + \lambda v_1 = 0. \quad (4)$$

Here, t and x are the time and propagation distance, scaled so that the group velocity of the electromagnetic waves in the fiber and Bragg reflectivity (i.e., essentially, the inverse Bragg-scattering length, x_B^{-1}) are normalized to be 1 (in physical units, $x=1$ and $t=1$ typically correspond to 1 mm and 10 ps, respectively), subscripts 1 and 2 are numbers of the two cores, and the strength of the linear coupling between them is measured by $\lambda = x_B/x_c$ (recall that x_c is the coupling length of the dual-core fiber). Accordingly, λ may be defined as real and positive. The amplitudes of the right- and left-traveling waves in each core, $u_{1,2}$ and $v_{1,2}$, are normalized so as to make the effective nonlinearity coefficient equal to 1 [as said above, in physical units the latter is, typically, $\sim 2\ (\mathrm{km\ W})^{-1}$ in ordinary fibers, while in PCFs it may be widely different], with the usual ratio of the SPM and XPM coefficients, 1:2.

If the grating is written on the second core with a spatial shift Δx relative to the first one, this gives rise to phase shifts $\pm\theta/2 \equiv \pm 2k\Delta x$ of the complex reflectivity coefficients in Eqs. (3) and (4), k being the carrier wave number of the counterpropagating electromagnetic waves. Since $\Delta x = \pi/k$ (i.e., Δx equal to the FBG period) corresponds to $\theta/2 = 2\pi$ and thus implies the absence of the actual mismatch, θ in Eqs. (1)–(4) may be restricted to interval $-\pi < \theta/2 < \pi$. Note that the complex conjugation, $\{u_{1,2}, v_{1,2}\} \to \{u_{1,2}^*, v_{1,2}^*\}$, followed by the spatiotemporal inversion, $\{x,t\} \to \{-x,-t\}$, transform the equations into themselves, with θ replaced by $-\theta$. Therefore it is sufficient to confine the analysis to the half interval, $0 \leqslant \theta/2 \leqslant \pi$.

Equations (1)–(4) admit an alternative interpretation in terms of the spatial-domain transmission of light [3,16]. In that case, the equations govern time-independent distributions of electromagnetic fields in parallel-coupled planar waveguides carrying diffraction gratings, with t and x playing the role of the propagation distance (z) and transverse coordinate, respectively (the diffraction grating is oriented along z). The phase shift corresponds to a mismatch in the mutual position of the gratings.

B. Spectrum (laboratory reference frame)

Linearization of Eqs. (1)–(4) gives rise to the following two branches of the dispersion relation for the plane-wave solutions, $u_{1,2}, v_{1,2} \sim \exp(ikx - i\omega t)$:

$$\omega^2 = 1 + \lambda^2 + k^2 \pm 2\lambda\sqrt{\cos^2(\theta/4) + k^2}. \quad (5)$$

A set of these relations, for different fixed values of λ and θ, is displayed in Fig. 1.

Straightforward analysis of Eq. (5) demonstrates that a band gap in the spectrum, in the form of $|\omega| < \omega_{\max}$, exists in *all cases*, except for $\theta=0$, $\lambda \geqslant 1$. However, two different generic situations are possible. If the coupling constant is small enough, $\lambda \leqslant \cos(\theta/4)$, the band gap's edge,

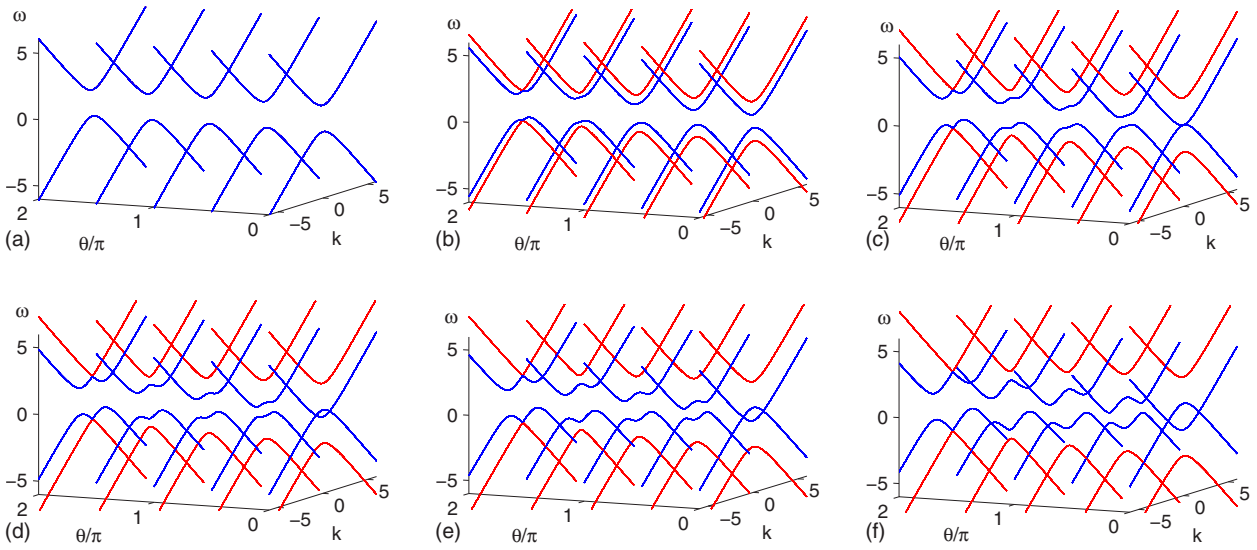

FIG. 1. (Color online) Evolution of pairs of dispersion curves (5) with the increase of mismatch θ between the linearly coupled gratings at fixed values of the coupling constant: $\lambda=0$, 0.5, 1, 1.25, 1.5, 2 [panels (a)–(f), respectively].

$$\omega^2 = \omega_{\max}^2 \equiv 1 + \lambda^2 - 2\lambda \cos(\theta/4), \tag{6}$$

is attained at $k=0$ (in the previously considered model with $\theta=0$ [8], this is the only possible case, as the gap does not exist at $\lambda>1$, if $\theta=0$). A different situation occurs at $\lambda > \cos(\theta/4)$. In this case, the edges, $|\omega(k)|=\omega_{\max}$, are attained at finite wave numbers,

$$k = k_{\text{edge}} = \pm\sqrt{\lambda^2 - \cos^2(\theta/4)}, \tag{7}$$

and $\omega_{\max}$ does not depend on λ, unlike its counterpart in Eq. (6):

$$\omega_{\max} = \sin(\theta/4). \tag{8}$$

The band gap's half width $\omega_{\max}$ is shown, as a function of λ and θ, in Fig. 2. This plot has its implications for the above-mentioned application of the dual-core fiber grating as the shear-stress sensor. In particular, the dependence of the gap's width on θ can be used for this purpose. Note that, the region of $\lambda > \cos(\theta/4)$, where the gap does not depend on λ, provides for the stability against inevitable fluctuations of the strength of the coupling between the cores (λ).

C. Spectrum in the moving reference frame

In the next section, it will be demonstrated that the system's band gap is always filled with solitons, in the laboratory or moving reference frame alike (i.e., there exists a GS for any value of ω belonging to the gap). Since quiescent Bragg solitons have not yet been created in the experiment (as mentioned above, currently available solitons have velocity $\geqslant 0.16$, in the present notation [6]), it is important to find a maximum velocity $c_{\max}$ up to which solutions for moving solitons exist in the present model (in the standard single-core model, $c_{\max}=1$ [17]). To this end, $c_{\max}$ should be found as the value of velocity c at which the gap shuts down in the moving reference frame, with independent variables $(\xi \equiv x - ct, t)$, instead of (x,t). Accordingly transformed equations (1)–(4) take the following form:

$$i(u_1)_t + i(1-c)(u_1)_\xi + (|u_1|^2/2 + |v_1|^2)u_1 + v_1 + \lambda u_2 = 0, \tag{9}$$

$$i(v_1)_t - i(1+c)(v_1)_\xi + (|v_1|^2/2 + |u_1|^2)v_1 + u_1 + \lambda v_2 = 0, \tag{10}$$

$$i(u_2)_t + i(1-c)(u_2)_\xi + (|u_2|^2/2 + |v_2|^2)u_2 + e^{i\theta/2}v_2 + \lambda u_1 = 0, \tag{11}$$

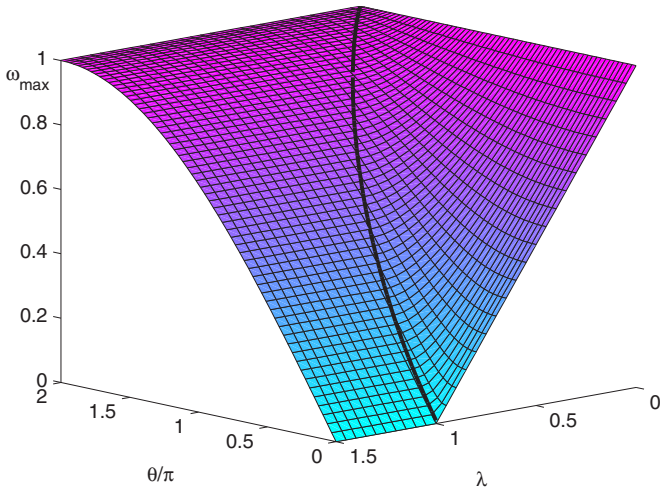

FIG. 2. (Color online) The size of the band gap in the linear spectrum of the coupled Bragg gratings with phase mismatch θ between them, $-\omega_{\max} < \omega < +\omega_{\max}$, is shown vs θ and coupling constant λ. The median line separates the λ-dependent $\omega_{\max}$, as given by Eq. (6), which is attained at $k=0$, and λ-independent $\omega_{\max}$ [given by Eq. (8)], which is attained at finite wave number k_{edge}, see Eq. (7). The band gap is absent ($\omega_{\max} \equiv 0$) in the case of $\theta=0$, $\lambda \geqslant 1$.

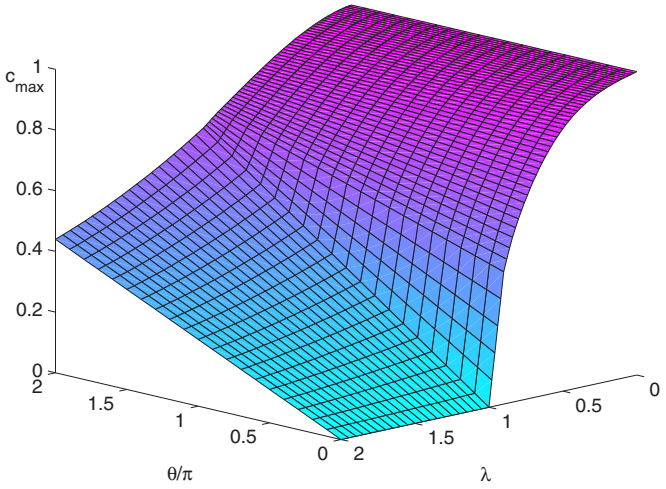

FIG. 3. (Color online) The largest velocity up to which the band gap exists in the moving reference frame. At $\theta=0$ and $\theta=2\pi$, dependences $c_{\max}(\lambda)$ are available in an analytical form; see Eqs. (14).

$$i(v_2)_t - i(1+c)(v_2)_\xi + (|v_2|^2/2 + |u_2|^2)v_2 + e^{-i\theta/2}u_2 + \lambda v_1 = 0. \tag{12}$$

The linearization of these equations leads to a Doppler-shifted variant of dispersion relation (5),

$$(\omega + ck)^2 = 1 + \lambda^2 + k^2 \pm 2\lambda\sqrt{k^2 + \cos^2(\theta/4)}. \tag{13}$$

The velocity at which the gap shuts down can be found in an explicit form from Eq. (13) in two limit cases, $\theta=0$ and $\theta=2\pi$:

$$c_{\max}^2(\theta=0) = 1-\lambda^2, \quad c_{\max}^2(\theta=2\pi) = (1+\lambda^2)^{-1}. \tag{14}$$

For the general case, $c_{\max}(\theta)$ was found numerically, see Fig. 3. Implications of these results for the experiment are obvious; in particular, the *increase* of $c_{\max}$ with θ opens a way to facilitate the creation of the solitons in the experiment, using the mismatch.

III. QUASISYMMETRIC AND ASYMMETRIC GAP SOLITONS

A. Previously known results

Stationary zero-velocity solutions to Eqs. (1)–(4) are sought for as

$$u_{1,2}(x,t) = e^{-i\omega t}U_{1,2}(x), \quad v_{1,2}(x,t) = e^{-i\omega t}V_{1,2}(x). \tag{15}$$

The substitution of this into Eqs. (1)–(4) leads to a set of four equations for functions $U_{1,2}(x)$ and $V_{1,2}(x)$, which admit a well-known reduction,

$$V_{1,2}(x) = -U_{1,2}^*(x). \tag{16}$$

With regard to the reduction, the remaining equations for $U_{1,2}(x)$ are

$$\omega U_1 + iU_1' + (3/2)|U_1|^2U_1 - U_1^* + \lambda U_2 = 0, \tag{17}$$

$$\omega U_2 + iU_2' + (3/2)|U_2|^2U_2 - e^{-i\theta/2}U_2^* + \lambda U_1 = 0, \tag{18}$$

where the prime stands for d/dx.

In the case of $\theta=0$, Eqs. (17) and (18) have obvious symmetric solutions, with $U_1=U_2\equiv U$, and asymmetric ones [8], that can be found in a numerical form, as well as semianalytically, by means of a variational approximation. The symmetric solitons obey the following equation:

$$(\omega+\lambda)U + iU' + (3/2)|U|^2U - U^* = 0, \tag{19}$$

which gives rise to a well-known family of exact solutions [17],

$$U(x) = \sqrt{\frac{2}{3}[1-(\omega+\lambda)^2]}\,\mathrm{sech}\left(x\sqrt{1-(\omega+\lambda)^2} - \frac{i}{2}\cos^{-1}(\omega+\lambda)\right). \tag{20}$$

The critical value of the coupling constant λ_c at which the symmetric GSs lose their stability through the symmetry-breaking bifurcation was found numerically (and also by means of the variational approximation) in Ref. [8]. For instance, $\lambda_c(\omega=0.75)=0.1462$, $\lambda_c(\omega=0.5)=0.2969$, and $\lambda_c(\omega=0)=0.5781$ (these particular values were actually found in the present work, see below). The symmetric GSs may be stable at $\lambda>\lambda_c$, where their AS counterparts do not exist. At $\lambda<\lambda_c$, the AS solitons exist and may be stable, while the symmetric solitons are definitely unstable.

In addition to the symmetric solitons, Eqs. (17) and (18) with $\theta=0$ also admit antisymmetric solutions, with $U_1=-U_2\equiv U$. The corresponding equation for $U(x)$ is Eq. (19) with λ replaced by $-\lambda$.

B. Soliton solutions in the phase-mismatched system

As said in the Introduction, in this work we aim to extend symmetric and asymmetric GSs, known at $\theta=0$ [8], to the phase-mismatched system of coupled FBGs, with $\theta>0$. We do not consider the extension of antisymmetric solutions, as they have a smaller chance to be stable. Indeed, in the small-amplitude limit, i.e., $1-(\omega+\lambda)^2\to 0$, exact solutions (20) become asymptotically equivalent to the usual nonlinear-Schrödinger solitons [18], and it is known that antisymmetric complexes of such solitons in the model of the ordinary dual-core fiber (without the grating) are unstable, while symmetric ones are stable, up to the point of the symmetry-breaking bifurcation [9].

The degree of the symmetry breaking in the two-component soliton may be quantified by means of parameter

$$\aleph \equiv \frac{A_1^2 - A_2^2}{A_1^2 + A_2^2}, \tag{21}$$

where A_1 and A_2 are amplitudes (maximum values) of fields $|U_1(x)|$ and $|U_2(x)|$ (by definition, we set $A_1^2 \geqslant A_2^2$). The first result revealed by numerical solutions of Eqs. (17) and (18) (the solutions were obtained by means of the standard finite-difference integration method) is that asymmetry parameter $\aleph$ remains equal to zero (within the numerical accuracy), up to a *bifurcation point* (see below), for the solitons obtained by continuation in θ of the symmetric solutions known in the exact form at $\theta=0$, see Eq. (20). Simultaneously, the energies

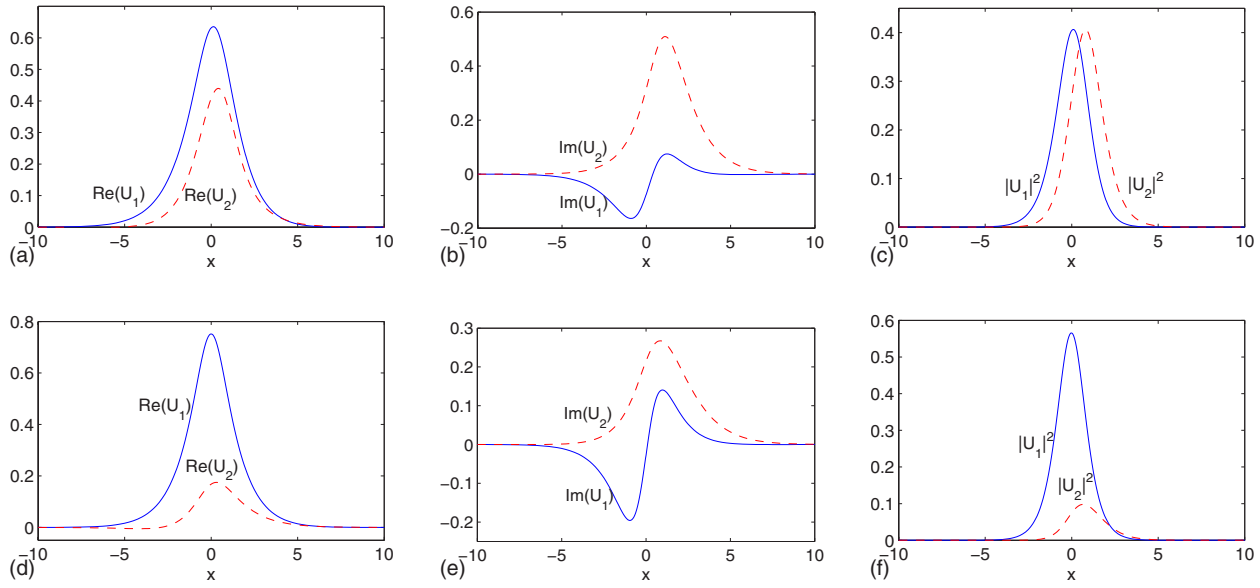

FIG. 4. (Color online) Typical examples of the quasisymmetric (a)–(c) and asymmetric (d)–(f) zero-velocity solitons which coexist, past the bifurcation point, at $\lambda=0.3$, $\theta=\pi$, and $\omega=0.5$ (for these values of θ and ω, the bifurcation value of the coupling constant is $\lambda_c \approx 0.4$). Panels (a) and (d), (b) and (e), and (c) and (f) display, respectively, real and imaginary parts and squared absolute values of fields $U_1(x)$ and $U_2(x)$, as found from the numerical solution of Eqs. (17) and (18).

of the two components, $E_{1,2}=\int_{-\infty}^{+\infty}|U_{1,2}(x)|^2dx$, *remain equal* for these solitons, which suggests to define the *energy asymmetry parameter*,

$$\aleph_E \equiv \frac{E_1 - E_2}{E_1 + E_2}, \tag{22}$$

as an alternative to the *power asymmetry* given by Eq. (21). Note that, for exact solution symmetric solutions (20), the total energy is

$$E \equiv \int_{-\infty}^{+\infty} [|U_1(x)|^2 + |U_2(x)|^2]dx = \frac{16}{3}\cos^{-1}(\omega + \lambda). \tag{23}$$

Numerical results demonstrate that $\aleph$ and $\aleph_E$ always vanish *simultaneously*, and we call the GS solutions (at $\theta \neq 0$) with $\aleph=\aleph_E=0$ *quasisymmetric* (QS) solitons. On the other hand, the symmetry-breaking bifurcation definitely continues too from $\theta=0$ to $\theta>0$, manifesting itself as a transition from the QS solitons to asymmetric (AS) ones, in which not only are the shapes of the U_1 and U_2 components not identical, but also the overall asymmetry parameters, $\aleph$ and $\aleph_E$, become different from zero (the component with a smaller amplitude, which we define as U_2, also has smaller energy).

We stress that the numerical results clearly demonstrate that the band gap is *completely filled* with solitons, i.e., at each value of the coupling constant and phase mismatch, λ and θ, and for each ω belonging to the band gap, as defined by Eqs. (6)–(8), it is possible to find the respective QS soliton, and, in addition, AS solutions are found too at each point beyond the bifurcation, i.e., at $\lambda<\lambda_c(\theta,\omega)$.

A typical example of a pair of the QS and AS gap solitons coexisting at a common set of parameters ($\lambda=0.3$, $\theta=\pi$, $\omega=0.5$), is presented in Fig. 4 (further analysis demonstrates that this AS soliton is stable, while its QS counterpart is unstable, all QS solitons being unstable past the bifurcation point, where their AS "rivals" exist). This example clearly shows that $\aleph=0$ for the QS soliton, although its shape is strongly asymmetric, while for the AS soliton, $\aleph=0.7046$.

The emergence of the AS soliton at the bifurcation point and evolution of its shape with the subsequent increase of the asymmetry are illustrated by Fig. 5. In this figure, the coupling parameter and phase mismatch are fixed, while the decrease of the soliton's frequency ω drives the growth of the asymmetry.

A noteworthy peculiarity obvious in Figs. 4 and 5 is that, at $\theta \neq 0$, the solitons break not only the symmetry between the components U_1 and U_2, but also the *spatial symmetry*, as manifested, in the QS and AS solitons alike, by separation between peaks of the two components. As this effect is entirely stipulated by the phase shift θ between the coupled

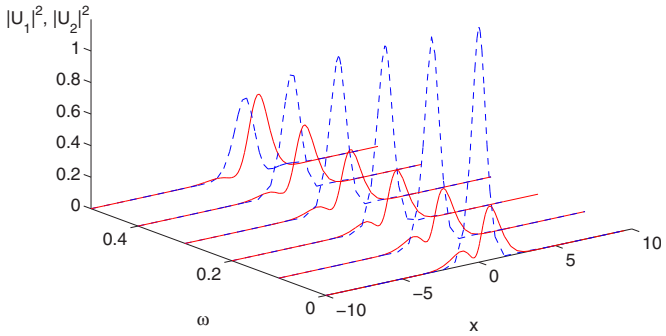

FIG. 5. (Color online) Evolution of the shape of the asymmetric zero-velocity soliton with the decrease of ω, at $\lambda=0.8$ and $\theta=3\pi/2$. The dashed and solid lines show $|U_1(x)|^2$ and $|U_2(x)|^2$, respectively. The asymmetric gap soliton splits off from the symmetric one at the bifurcation point $\omega_c=0.4425$.

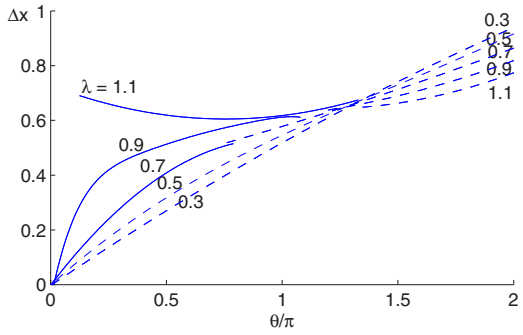

FIG. 6. (Color online) Separation (Δx) between centers of two components, $|U_1(x)|$ and $|U_2(x)|$, of the zero-velocity gap solitons with $\omega=0$ vs the phase mismatch θ between the coupled gratings, for several different values of the coupling constant λ. Continuous and dashed lines show the dependence for the quasisymmetric and asymmetric solitons, respectively.

FBGs, it is natural to display the separation as a function of θ, as done in Fig. 6 (the curve corresponding to $\lambda=1.1$ terminates at finite θ as the gap does not exist at $\theta=0$ for $\lambda>1$, see Fig. 3).

Figure 5 also demonstrates that the breaking of the spatial symmetry may lead to appearance of an extra "hump" (local maximum) in the profile of $|U_2(x)|$ in AS solitons (recall that, for solitons of this type, U_2 is defined as the component with a smaller amplitude), but only on *one side* of the main peak in the shape of $|U_2(x)|$. Some QS solitons also feature extra humps, but in that case, *each component* develops an additional hump, and in the two components they are located on opposite sides. These results are noteworthy, as double-humped structures are *never* featured by GSs (symmetric or asymmetric ones) in the earlier studied symmetric dual-core model, with $\theta=0$, as well as in the standard single-core one [8,17].The observation double-humped solitons in the mismatched dual-core FBG may be a challenge to the experiment.

Shapes of moving solitons are generally similar to those displayed above, with one essential difference: since reduction (16) is not valid for the moving solitons, they are described by four field profiles, $|u_{1,2}(\xi)|$ and $|v_{1,2}(\xi)|$ (recall $\xi \equiv x-ct$). As an example, an array of shapes of moving solitons is displayed in Fig. 7.

IV. BIFURCATION DIAGRAMS FOR TRANSITIONS BETWEEN QUASISYMMETRIC AND ASYMMETRIC SOLITONS

Bifurcation diagrams which account for transitions between the QS and AS solutions were drafted by scanning the relevant parameter space, $(\lambda, \theta, \omega)$, inside the band gap. A basic form of the diagram shows asymmetry parameter $\aleph$, defined in Eq. (21), as a function of coupling constant λ, at fixed values of the mismatch and soliton's frequency, θ and ω, see Fig. 8 (the diagrams for $\theta=0$ are identical to those reported in Ref. [8]). The figures do not show the range of $\omega<0$, as in this case all solitons are unstable, as shown in the next section.

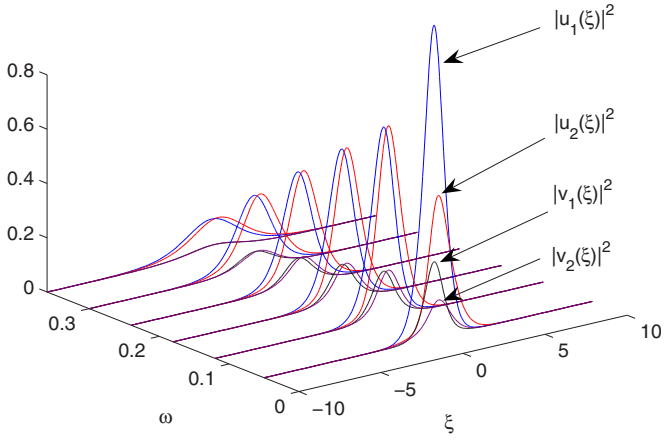

FIG. 7. (Color online) Several examples of stable solitons moving at velocity $c=0.6$, in the system with $\theta=\pi$ and $\lambda=0.5$, obtained from numerical solution of Eqs. (9)—(12). The solitons are shown for values of the intrinsic frequency (defined in the moving reference frame) which vary between $\omega=0.05$ and $\omega=0.36$.

The bifurcation diagrams in Fig. 8(a) show a typical *supercritical* transition from QS to AS solitons, qualitatively similar to that discovered in Ref. [8] for the model with $\theta=0$. However, jumps between the QS and AS solution branches, observed in Figs. 8(b) and 8(c) with the increase of θ, strongly suggest that the supercritical bifurcation goes over into a *subcritical* one, an assumed form of which is depicted in Fig. 8(d). Recall that a subcritical bifurcation, although close to a supercritical one (i.e., with a small hysteretic interval) was discovered in the study of two-component solitons in the system of two linearly coupled nonlinear Schrödinger equations, describing an ordinary dual-core nonlinear optical fiber (without gratings) [9]. Our numerical method could not provide for convergence of stationary solutions close to the conjectured turning point, which is amenable for the jumps in Figs. 8(b) and 8(c).

For moving solitons, the bifurcation diagrams seem qualitatively similar, as illustrated by a typical set displayed in Fig. 9. In this figure, the diagrams are presented in terms of both the peak-power and energy asymmetry parameters, $\aleph$ and $\aleph_E$, which are defined similarly to their counterparts for the zero-velocity solitons, cf. Eqs. (21) and (22), but taking into regard that $|u_{1,2}| \neq |v_{1,2}|$ for moving solitons:

$$\aleph \equiv \frac{(A_1^2+B_1^2)-(A_2^2+B_2^2)}{(A_1^2+B_1^2)+(A_2^2+B_2^2)}, \tag{24}$$

$$\aleph_E \equiv \frac{\int_{-\infty}^{+\infty}\{[|u_1(\xi)|^2+|v_1(\xi)|^2]-[|u_2(\xi)|^2+|v_2(\xi)|^2]\}d\xi}{\int_{-\infty}^{+\infty}\{[|u_1(\xi)|^2+|v_1(\xi)|^2]+[|u_2(\xi)|^2+|v_2(\xi)|^2]\}d\xi}, \tag{25}$$

where $A_{1,2}$ and $B_{1,2}$ are the values of $|u_{1,2}|$ and $|v_{1,2}|$ at the point where the soliton's power, $|u_1(\xi)|^2+|v_1(\xi)|^2+|u_2(\xi)|^2+|v_2(\xi)|^2$, attains its peak (maximum) value.

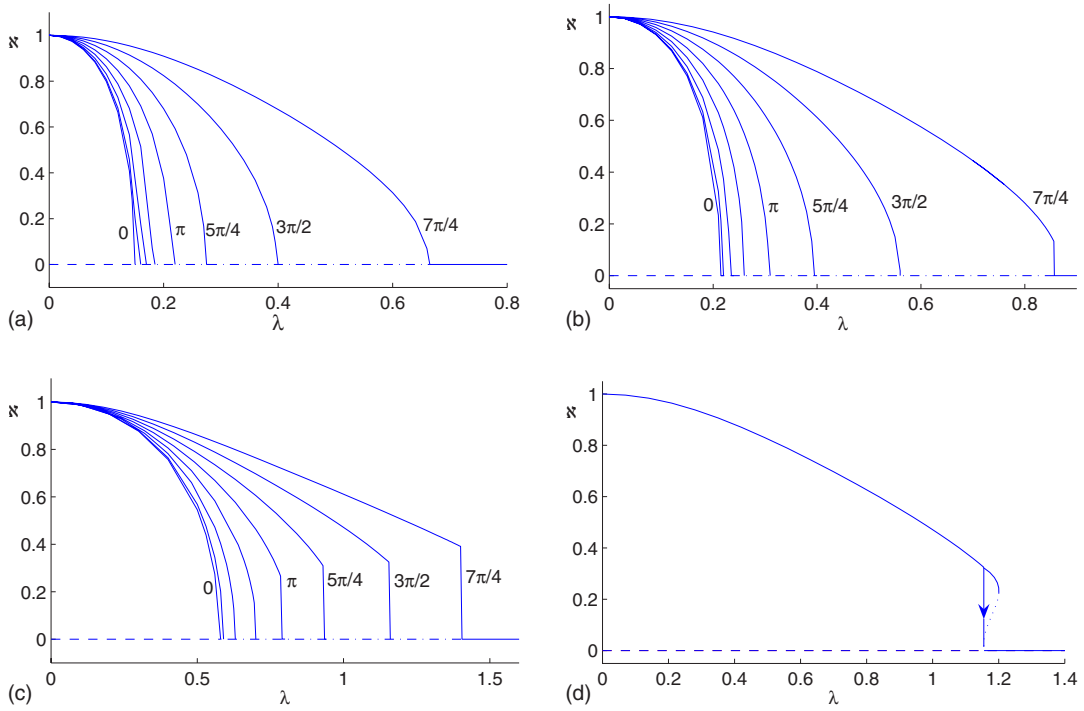

FIG. 8. (Color online) A set of bifurcation diagrams, showing the asymmetry parameter ($\aleph$), defined as per Eq. (21), vs the coupling constant λ at fixed values of the phase mismatch between the coupled gratings, $\theta=0,\pi/4,\ldots,7\pi/4$, and at three different fixed values of the soliton's intrinsic frequency, (a) $\omega=0.75$, (b) $\omega=0.64$, and (c) $\omega=0$. Solution branches with $\aleph=0$ and $\aleph>0$ correspond to quasisymmetric and asymmetric solitons, respectively. Panel (d) shows the conjectured full form of the *subcritical bifurcation diagram* underlying the pictures shown in panel (c), its continuation to the right of the vertical arrow being a part which plausibly exists, but was not found due to difficulties with the convergence of the numerical procedure. Segments of the latter part above and below the turning point must be stable and unstable, respectively.

Getting back to the zero-velocity solitons, a global description of the bifurcations is provided by Fig. 10. Panel (a) shows the critical value of the soliton's frequency ω_c at which the bifurcation takes place, as a function of the coupling constant λ at several fixed values of mismatch θ, and panel (b) additionally displays the corresponding critical coupling constant λ_c vs θ at several fixed values of ω. In either case, both QS and AS solitons exist beneath the respective critical lines, while only QS solitons are found in regions above the lines.

V. STABILITY OF THE GAP SOLITONS

Stability of the quiescent and moving solitons of both types, quasisymmetric and asymmetric, was tested in direct simulations of the evolution of perturbed solitons. The results can be summarized in a simple form. First of all, the QS solitons are stable against asymmetric perturbations before the bifurcation, when AS solutions do not exist. As soon as the latter emerge, the QS soliton loses its stability and, in direct simulations, it transforms itself into a breather, which features strong breaking of the symmetry between the components and gradual relaxation to an expected AS soliton, see a typical example in Fig. 11. On the other hand, AS solitons, if they exist, never feature instability towards returning to the QS shape. These stability properties are essentially the same as reported, for the model with $\theta=0$, in Ref. [8].

Exact stability features may be different in a narrow vicinity of the conjectured subcritical bifurcation, see Figs. 8(b) and 8(c), where one may expect bistability and hysteresis, due to coexistence of stable QS and AS solitons. Accurate investigation of this issue would have little practical impact, as the expected bistability or hysteretic interval will be very narrow, cf. the situation in the model of ordinary dual-core nonlinear optical fibers [9].

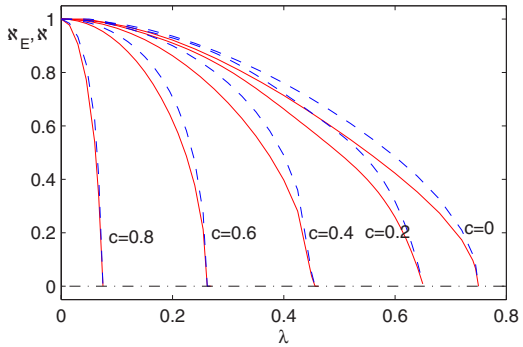

FIG. 9. (Color online) A set of bifurcation diagrams for moving solitons at several different values of velocity c. The plots show the energy and peak-power asymmetry parameters, $\aleph_E$ and $\aleph$, which are defined as per Eqs. (24) and (25), vs the coupling constant λ at fixed mismatch and intrinsic frequency, $\theta=1.5\pi$ and $\omega=0.5$. At all values of c, the curve for $\aleph_E$ is located to the left of its counterpart showing $\aleph$, but they originate in exactly the same bifurcation point.

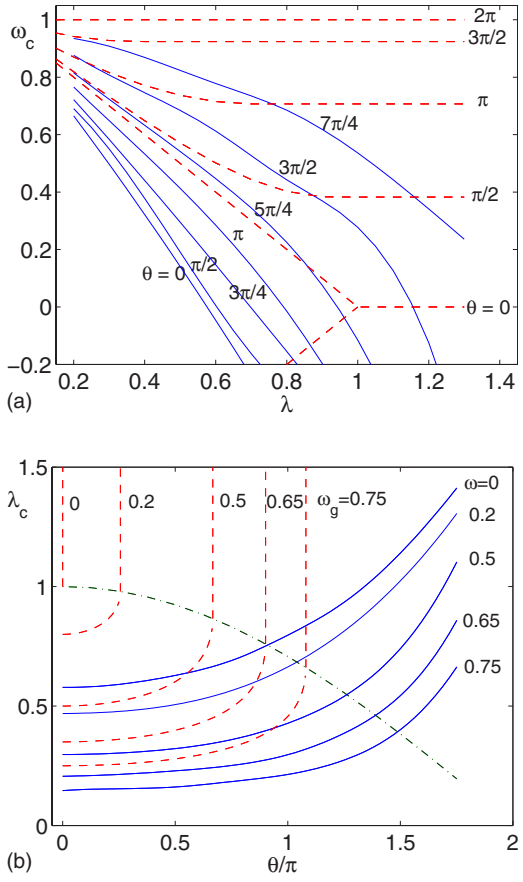

FIG. 10. (Color online) (a) Frequency ω of the zero-velocity soliton at the bifurcation point vs the coupling constant λ at several fixed values of the phase mismatch θ. (b) The value of λ at the bifurcation point vs θ, at several different fixed values of ω. In panels (a) and (b), dashed lines show upper borders of the band gap for different values of θ and ω, respectively. In panel (a), both upper and lower band-gap borders are shown for $\theta=0$; they coalesce into a single line at $\lambda>1$, as the gap does not exist in that case. The transversal dashed-dotted line in panel (b) shows the border, $\lambda=\cos(\theta/4)$, between cases when the band gap's edge is attained at $k=0$, which corresponds to Eq. (6), or at finite k [see Eq. (7)], which corresponds to Eq. (8). Results for $\omega<0$ are not included, as the solitons with negative frequencies are unstable.

It is known that GSs, even in the standard models of the single-core grating, may be unstable against oscillatory perturbations corresponding to complex eigenvalues. This instability was predicted by means of the variational approximation in Ref. [14], and then investigated by means of accurate numerical methods [15]. It was concluded that the zero-velocity GS, given by exact solution (20) with $\lambda=0$, is stable for $\omega>\omega_{\min}\simeq-0.015$, and unstable against oscillatory perturbations otherwise. For practical purposes, it may be assumed that the stability region is $\omega\geqslant 0$. It was also shown that, for moving solitons, the dependence of the stability border on velocity c is very weak, hence $\omega=0$ may be adopted as the stability border for $c\neq 0$ too.

We have tested the full stability of QS and AS solitons, which are expected to be stable against symmetry-breaking perturbations (i.e., QS solitons when their AS counterparts do not exist, and the AS solitons otherwise). Adding arbitrary initial perturbations, we have concluded that these solitons are stable indeed if their intrinsic frequency is *positive*, $\omega\geqslant 0$, and unstable for $\omega<0$, as shown in Fig. 12 [note the multihumped shape of the stable solitons displayed in Figs. 12(b) and 12(c)]. Figure 12(a) suggests that the instability tends to completely destroy solitons which are unstable against oscillatory perturbations.

As an additional illustration of the stability of solitons with $\omega\geqslant 0$, in Fig. 13 we show the evolution of a perturbed AS soliton in the system with the maximum mismatch, $\theta=2\pi$. The corresponding unperturbed AS soliton features the double-humped structure in its component u_2 in the most salient form, as the two humps have equal heights, in this case. Such solitons are of special interest, as they are drastically different from the ordinary (always single-humped) GSs found in the model of the single-core FBG [17] or its dual-core counterpart with zero mismatch [8].

As concerns the moving solitons, general principles controlling their stability were found (in systematic simulations) to be the same as for their quiescent counterparts. In particular, the moving QS solitons are stable against the symmetry breaking as long as AS solutions do not exist, and unstable otherwise, while the moving AS solitons are always stable against perturbations of this type. The condition for the sta-

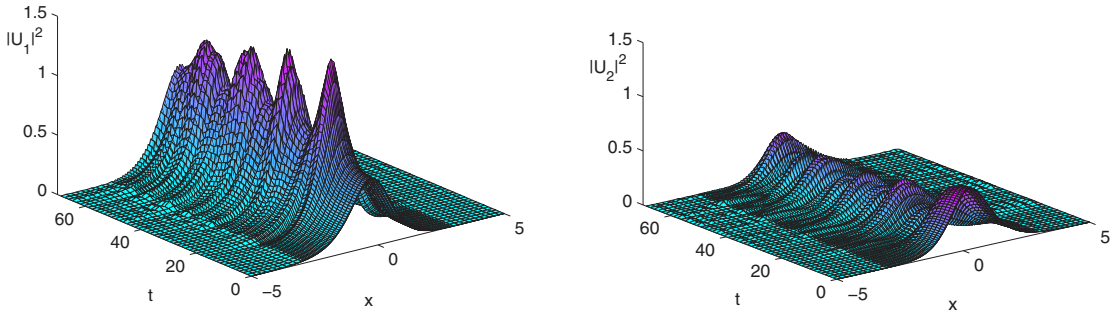

FIG. 11. (Color online) A typical example of the instability of a quasisymmetric quiescent soliton past the bifurcation point, for $\lambda=0.5$, $\theta=3\pi/4$, and $\omega=0.2$ [λ is slightly smaller than the respective bifurcation value, $\lambda_c(\theta=3\pi/4,\omega=0.2)=0.5633$]. The spontaneous symmetry breaking makes one component larger (a), and one smaller (b).

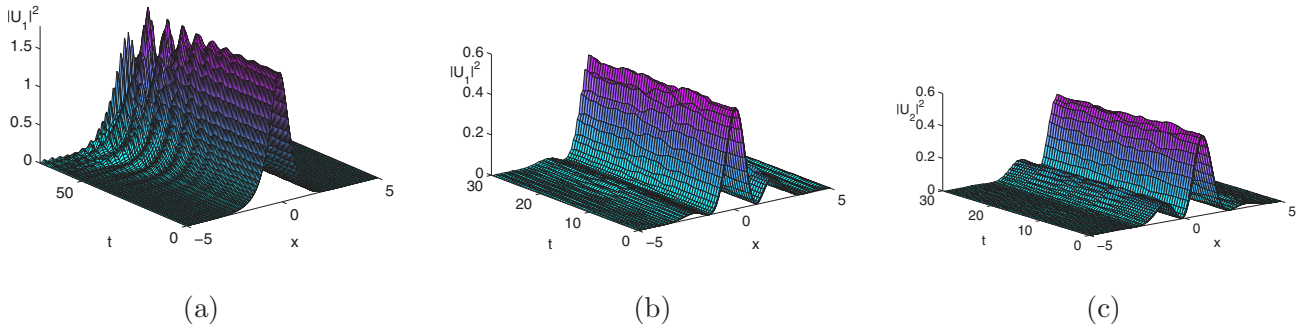

FIG. 12. (Color online) (a) An example of the destruction of an asymmetric soliton with a negative intrinsic frequency ($\omega=-0.3$) by the oscillatory instability, at $\lambda=0.5$ and $\theta=\pi$. Only the u_1 component is shown, as the evolution of its u_2 counterpart is similar. (b) and (c) Stability of both components of a quasisymmetric soliton with $\omega=0.65$, $\lambda=1.3$, and $\theta=7\pi/4$.

bility of all the solitons against oscillatory perturbations is again $\omega \geqslant 0$, up to the accuracy of the simulations (for moving solitons, the accuracy in the identification of the instability threshold is somewhat lower than for the quiescent ones).

VI. CONCLUSIONS

We have introduced a generalized model of two linearly coupled waveguides carrying Bragg gratings with the phase mismatch θ between the gratings. The model may be realized in the temporal domain, in the form of a dual-core fiber grating, and in the spatial domain, assuming a pair of two parallel-coupled planar waveguides with diffraction gratings. For $\theta=0$, the symmetry-breaking bifurcation of GSs (gap solitons) in this model was investigated before. In this work, we examine how the mismatch between the linearly coupled gratings modifies families of symmetric and asymmetric GSs, and how it affects the bifurcation between them. The spectrum of the linearized version of the model was found in an analytical form, and numerical results demonstrate that the corresponding band gap is completely filled with solitons. The maximum velocity of moving solitons was found too, a noteworthy finding being that the maximum velocity *increases* with θ, which suggests a possibility to create *faster* Bragg solitons in the experiment. Another noteworthy effect induced by the mismatch is the fact that the band-gap's width does not depend on the coupling strength λ if λ exceeds a minimum value [$\lambda_{\min}=\cos(\theta/4)$, in the present notation]. Irrespective of the solitons, the proposed setting may find an application to the design of sensors measuring the shear stress, through the mismatch induced by the stress in the dual-core grating.

Finite θ transforms the symmetric GS into quasisymmetric (QS) ones, whose peak powers and energies remain equal. In addition, $\theta \neq 0$ breaks the spatial symmetry of the soliton, introducing a finite separation between peaks in its two components. In the general case, it also gives rise to extra hump(s) in the profiles of one or both components (in the AS and QS solitons, respectively).

The QS solitons are stable against symmetry-breaking perturbations as long as asymmetric (AS) solutions do not exist. If θ is small, AS solitons emerge from the QS branch as stable states through a supercritical bifurcation, simultaneously destabilizing the QS solitons. However, the bifurcation becomes *subcritical* at larger θ. The change of the character of the bifurcation, controlled by the mismatch between the gratings, was not found in previously studied models.

The stability of both the QS and AS solitons against oscillatory perturbations (which are not related to the symmetry breaking) proves to be the same as in the previously studied model with $\theta=0$: the solitons are unstable, in this sense, if their intrinsic frequency is negative, $\omega<0$. Finally, properties (bifurcations and the stability) of moving solitons are qualitatively similar to those found in their quiescent counterparts.

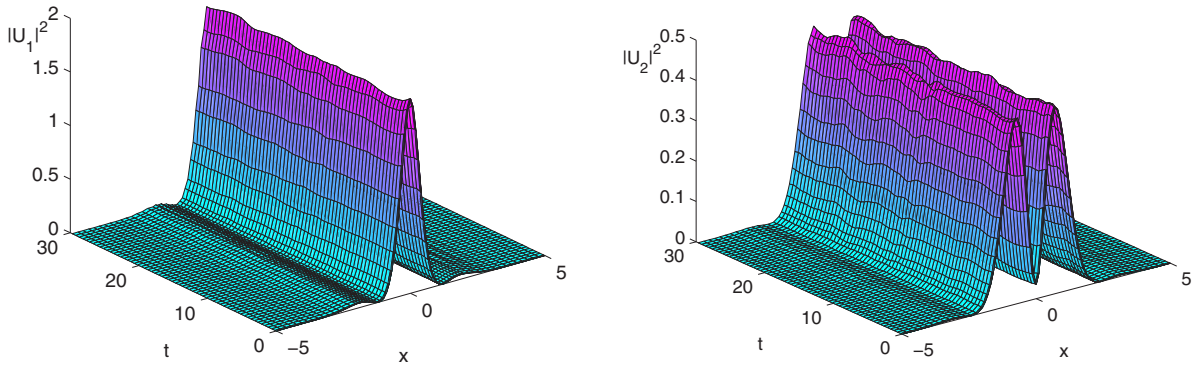

FIG. 13. (Color online) Stable evolution of a perturbed asymmetric soliton featuring the spatially symmetric double-humped structure in its component u_2, for $\omega=0$, $\lambda=1.3$, and $\theta=2\pi$.

[1] R. Kashyap, *Fiber Bragg Gratings* (Academic, San Diego, 1999).
[2] C. M. de Sterke and J. E. Sipe, Prog. Opt. **33**, 203 (1994).
[3] A. Y. Cho, A. Yariv, and P. Yeh, Appl. Phys. Lett. **30**, 471 (1977).
[4] Y. S. Kivshar and G. P. Agrawal, *Optical Solitons* (Academic, San Diego, 2003).
[5] B. J. Eggleton, R. E. Slusher, C. M. de Sterke, P. A. Krug, and J. E. Sipe, Phys. Rev. Lett. **76**, 1627 (1996).
[6] B. J. Eggleton, C. M. De Sterke, and R. E. Slusher, J. Opt. Soc. Am. B **16**, 587 (1999).
[7] J. T. Mok, C. M. De Sterke, I. C. M. Litter, and B. J. Eggleton, Nat. Phys. **2**, 775 (2006).
[8] W. Mak, B. A. Malomed, and P. L. Chu, J. Opt. Soc. Am. B **15**, 1685 (1998).
[9] N. Akhmediev and A. Ankiewicz, Phys. Rev. Lett. **70**, 2395 (1993); P. L. Chu, B. A. Malomed, and G. D. Peng, J. Opt. Soc. Am. B **10**, 1379 (1993); B. A. Malomed, I. M. Skinner, P. L. Chu, and G. D. Peng, Phys. Rev. E **53**, 4084 (1996).
[10] M. Åslund, L. Poladian, J. Canning, and C. M. de Sterke, J. Lightwave Technol. **20**, 1585 (2002).
[11] W. N. MacPherson, J. D. C. Jones, B. J. Mangan, J. C. Knight, and P. St. J. Russell, Opt. Commun. **223**, 375 (2003).
[12] A. A. Sukhorukov and Y. S. Kivshar, Phys. Rev. Lett. **97**, 233901 (2006).
[13] C. Cambournac, T. Sylvestre, H. Maillotte, B. Vanderlinden, P. Kockaert, Ph. Emplit, and M. Haelterman, Phys. Rev. Lett. **89**, 083901 (2002).
[14] B. A. Malomed and R. S. Tasgal, Phys. Rev. E **49**, 5787 (1994).
[15] I. V. Barashenkov, D. E. Pelinovsky, and E. V. Zemlyanaya, Phys. Rev. Lett. **80**, 5117 (1998); A. De Rossi, C. Conti, and S. Trillo, *ibid.* **81**, 85 (1998).
[16] J. Feng, Opt. Lett. **18**, 1302 (1993); R. F. Nabiev, P. Yeh, and D. Botez, *ibid.* **18**, 1612 (1993).
[17] A. B. Aceves and S. Wabnitz, Phys. Lett. A **141**, 37 (1989); D. N. Christodoulides and R. I. Joseph, Phys. Rev. Lett. **62**, 1746 (1989).
[18] N. M. Litchinitser, B. J. Eggleton, and D. B. Patterson, J. Lightwave Technol. **15**, 1303 (1997).